Article

Shear Behavior of Concrete Encased Steel Truss Composite Girders

Chisung Lim [1] , Seung-Ho Choi [2], Jae Yuel Oh [3], Sun-Jin Han [2] , Moon-Sung Lee [4] and Kang Su Kim [5,*]

1   Korea Authority of Land & Infrastructure Safety 24, Ena-ro 128beon-gil, Jinju-si 52856, Korea;
    ychs4618@kalis.or.kr
2   Department of Architectural Engineering, University of Seoul, 163 Seoulsiripdae-ro, Dongdaemun-gu,
    Seoul 02504, Korea; ssarmilmil@gmail.com (S.-H.C.); sjhan1219@gmail.com (S.-J.H.)
3   Sejin R&S 19, Seongsuil-ro, Seongdong-gu, Seoul 04779, Korea; hahappyppy@naver.com
4   School of Architecture & Architectural Engineering, Hanyang University, Erica 55 Hanyangdaehak-ro,
    Sangrok-gu, Ansan 15588, Korea; moonlee@hanyang.ac.kr
5   Department of Architectural Engineering and Smart City Interdisciplinary Major Program,
    University of Seoul, 163 Seoulsiripdae-ro, Dongdaemun-gu, Seoul 02504, Korea
*   Correspondence: kangkim@uos.ac.kr; Tel.: +82-2-6490-2762; Fax: +82-2-6490-5509

Abstract: In this study, experimental tests were performed to evaluate the shear performance of encased steel truss (EST) composite girders that can resist loads at construction and composite stages. Four full-scale EST composite girders were fabricated, where the truss type (Pratt truss and Warren truss) and presence of stirrups were set as main test variables. The test results showed that in specimens applied with the Pratt truss, horizontal shear cracking occurring along the interface between concrete and steel was the dominant failure mode. Based on the crack pattern and failure plane observed from the test, the horizontal shear strengths of the Pratt truss specimens were calculated, which provided conservative results. On the other hand, in the specimens with the Warren truss inside, the strengths of the specimens were governed by the shear failure occurring in the screw rod connecting the truss elements prior to the yielding of the diagonal member. The shear strengths of the Warren truss specimens calculated based on the shear failure of the screw rod were similar to that obtained from the test.

Keywords: concrete encased beam; composite; shear; horizontal shear; truss

1. Introduction

Composite structural systems are widely used in construction sites because they afford long spans and reduced floor heights. In this regard, steel–concrete composite members with structural performance improved by efficiently utilizing the advantages of concrete and steel [1–7], prestressed concrete members with flexural and shear performance improved by introducing prestress into concrete with low tensile strength [8–10], and composite members applied with fibers and high-performance materials [11–19] have been developed hitherto.

De Sutter et al. [5] conducted shear tests on hybrid composite-concrete beams and analyzed changes in principal strain and stress orientations under loading conditions through strain analysis. Monti and Petrone [2] proposed shear capacity equations for composite truss beams and verified their proposed model based on nonlinear analysis and experiments. Ayyub et al. [6,7] experimentally verified the resistance performance of prestressed steel–concrete composite members against positive/negative moments and suggested a linear analysis method for prestressed steel–concrete composite girders based on their experimental results. Khuntia et al. [12] obtained shear test results of reinforced concrete members incorporating normal or high-strength fibers through a literature review and proposed a shear strength equation suitable for fiber-reinforced concrete based on the shear database collected. Di et al. [17] performed monotonic push-out tests of glass

fiber reinforced polymer (GFRP) girders—in which various types of connections were set as key variables—to identify the bond performance between GFRP girders and concrete slabs. Based on the test results, Di et al. reported that the use of connections with single T-shaped and slotted perforated plates resulted in high load-carrying capacity and that the transverse rebar could enhance the ultimate bearing capacity and ductility. Dunaj et al. [18] proposed a method for finite element modeling of the dynamic properties of steel–polymer concrete beams, and their model showed a good accuracy in the evaluation of the natural frequencies and mode shapes obtained from their experiments.

Meanwhile, although studies regarding composite members have actively been conducted in recent years, the demand for a composite structural system demonstrating excellent structural performance while ensuring economic feasibility and constructability is still prevalent in the construction market. Accordingly, in South Korea, encased steel truss (EST) composite girders with steel trusses embedded in concrete have been developed recently, as shown in Figure 1. In the EST composite system, the truss member supports the formwork self-weight and construction load, thereby minimizing temporary work processes, such as shore installation. Figure 1a shows the EST composite girder. The steel truss fabricated in a plant comprises top and bottom chords as well as transverse and diagonal members. Furthermore, the truss and external formwork are installed at the site. After cast-in-place (CIP) concrete is poured and cured, grout is injected into the truss connection, as shown in Figure 1b. Figure 2 shows the connection details of the EST composite system. The bolt hole with a diameter of 18 mm was drilled at the end of the truss members and penetrated through a screw rod of 15.9 mm in diameter and 400 MPa yield strength; subsequently, the chord and diagonal members were fastened together using D-corn and bolts. The D-corns, which served as a spacer between the diagonal members and the form, were removed after the concrete was poured and cured, and subsequently the remaining space was filled with mortar. In the EST composite girder, an efficient load transfer was possible because the top and bottom chords of the truss resisted compressive and tensile forces due to bending moments, whereas the transverse and diagonal members as well as concrete resisted shear forces.

The aim of this study was to verify the shear performance of the EST composite girder. Hence, the truss type (Pratt truss and Warren truss) and presence of stirrups were set as the main test variables, and shear tests were performed subsequently. The crack patterns and shear-force–displacement behaviors of the specimens were analyzed in detail. Based on the failure mode of the specimen, the shear strength of the EST composite girder was calculated considering the horizontal shear performance between the EST and concrete; subsequently, it was verified based on a comparison with the test results. Through this study, it clearly appeared that the proposed method provided good evaluation results on the shear strengths of EST composite girder specimens in a conservative manner, and thus it is worth applying to practical design.

The structure of this paper is as follows: In the Experimental Program section, the specimen details and loading apparatus are summarized, and the shear behaviors of specimens including failure modes and crack patterns are reported in detail. The next section summarizes the evaluations of the shear strengths of specimens that were conducted, considering the horizontal shear failure of embedded steel truss and the strength of the truss node, and the test and evaluation results are compared and discussed. In the Conclusions section, the main research findings of this study are summarized and additional experimental works are suggested for future research.
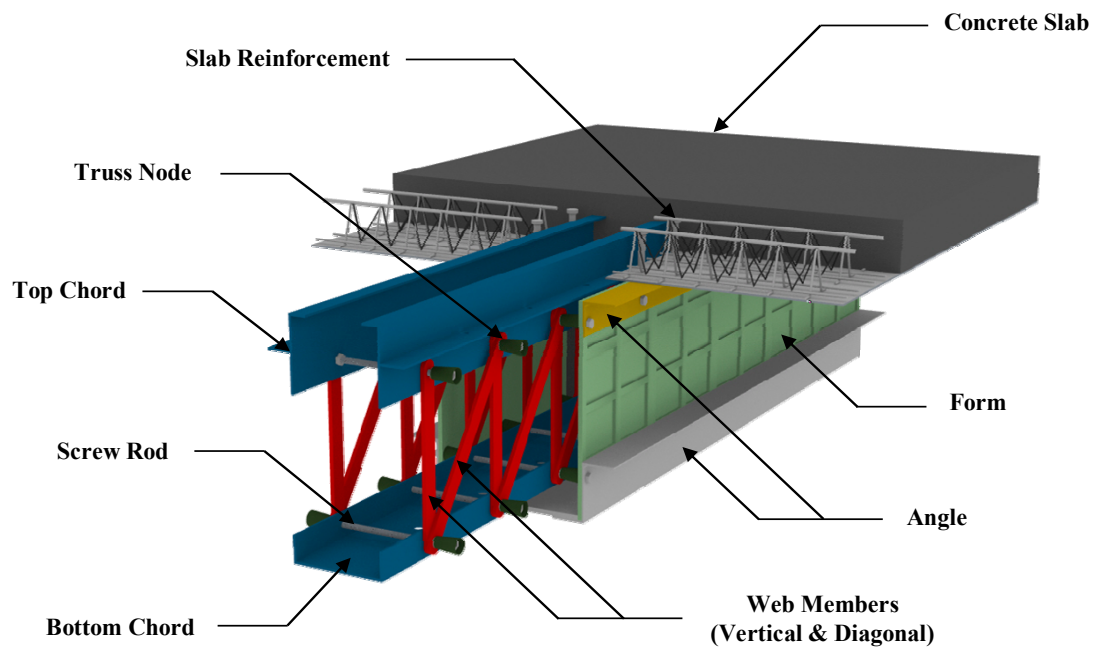
(**a**) EST composite girder at construction stage
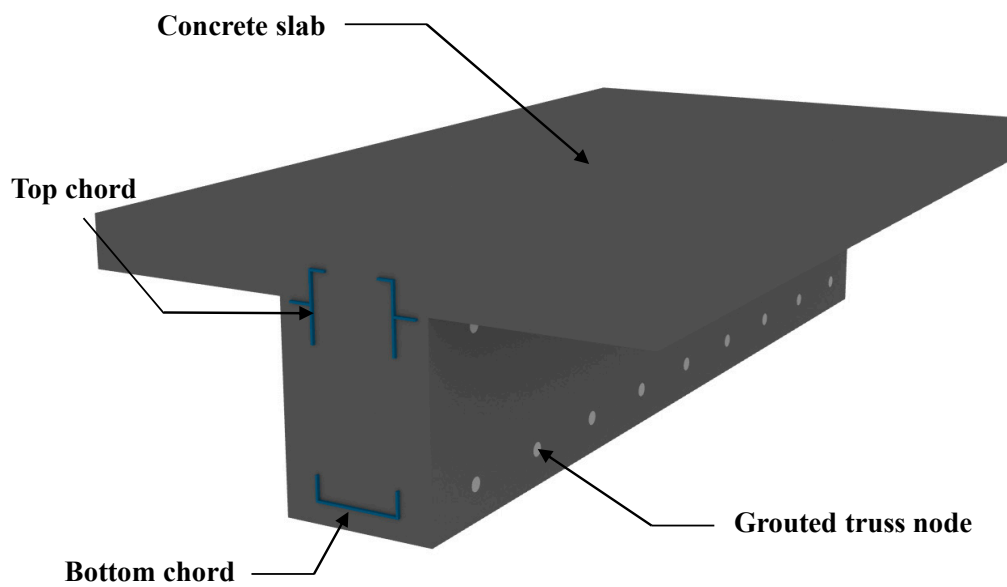
(**b**) EST composite girder after composite with cast-in-place concrete

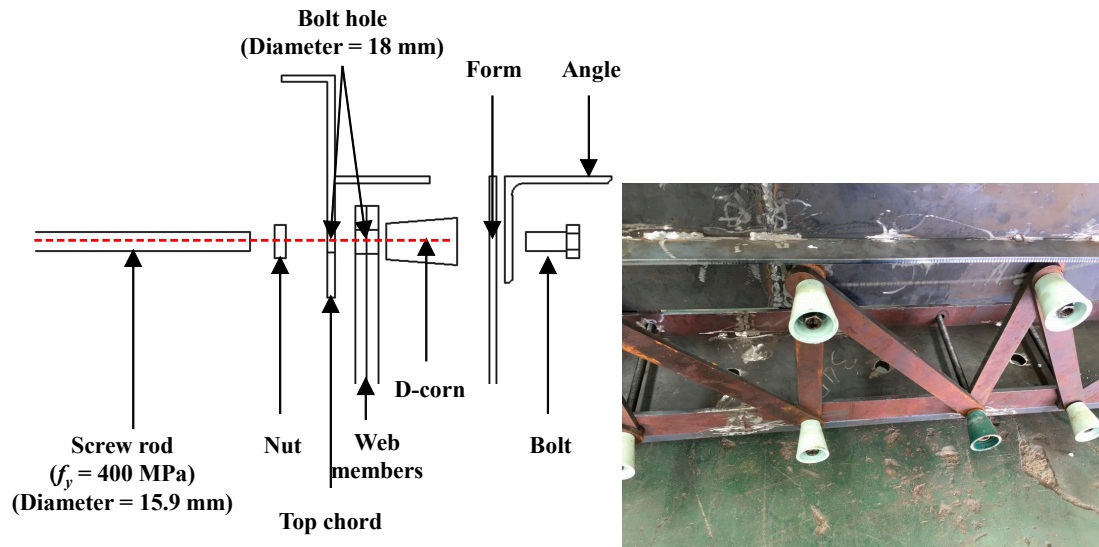**Figure 1.** Schematic description of encased steel truss (EST) composite girder.

Figure 2. Connection details at truss node.

2. Experimental Program

2.1. Test Specimens

　　To identify the shear performance of EST composite girders, four full-scale specimens were fabricated to conduct a test. As shown in Table 1, the truss type (Pratt truss (P) and Warren truss (W)) and the presence of stirrups were set as main test variables. Reinforcing bars of 13 mm in diameter were used for the stirrups, and 25-mm-diameter rebars were used as tensile reinforcements. Figure 3 shows the details of the P-specimen series (specimen PV, specimen P) to which the Pratt truss was applied. In addition, PV and P represent the specimens with and without vertical stirrups, respectively. As shown in Figure 3a, the Pratt truss was composed of top and bottom chords as well as vertical and diagonal web members; furthermore, vertical shear reinforcements were placed at 300 mm intervals in the PV specimen, as shown in Figure 3b. In addition, six D25 tensile reinforcements were placed to prevent flexural failure and induce shear failure, and the thickness of the bottom chord was 20 mm. The bottom chord was considered as tensile reinforcement in the calculation of flexural strengths of the specimens. As shown in Figure 3c, the stirrup was not placed in the P specimen, and four D25 tensile reinforcements were placed on the tension side of the section. Except for the presence of stirrups and the tensile reinforcement placement, all the section details were the same for both specimens. The side cover thickness of the top chord, which corresponds to the resistance surface of concrete against horizontal shear, was 40 mm, whereas the top cover thickness was 65 mm. Meanwhile, the side cover thickness of the bottom chord was 72 mm, whereas the bottom cover thickness was 50 mm.

Table 1. Details of test specimens.

Specimen	PV [a]	Pb [b]	WV [c]	W [d]
Truss type	Pratt		Warren	
Concrete compressive strength (MPa)		29.7		
Width × Height (mm)	500 × 600	500 × 600	500 × 600	500 × 600
Thickness of bottom chord (mm)	20	20	20	16
Longitudinal reinforcement	6-D25	4-D25	-	-
Web members (Vertical)	PL–40 × 6 @ 300	PL–40 × 6 @ 300	-	-
Web members (Diagonal)	PL–40 × 6 @ 300	PL–40 × 6 @ 300	PL–40 × 6 @ 400	PL–40 × 6 @ 400
Stirrups	2-D13@300		2-D13@400	

[a] PV = Pratt truss with vertical stirrups; [b] P = Pratt truss without vertical stirrups. [c] WV = Warren truss with vertical stirrups; [d] W = Warren truss without vertical stirrups.

(**a**) Truss arrangement

(**b**) Section details of PV specimen

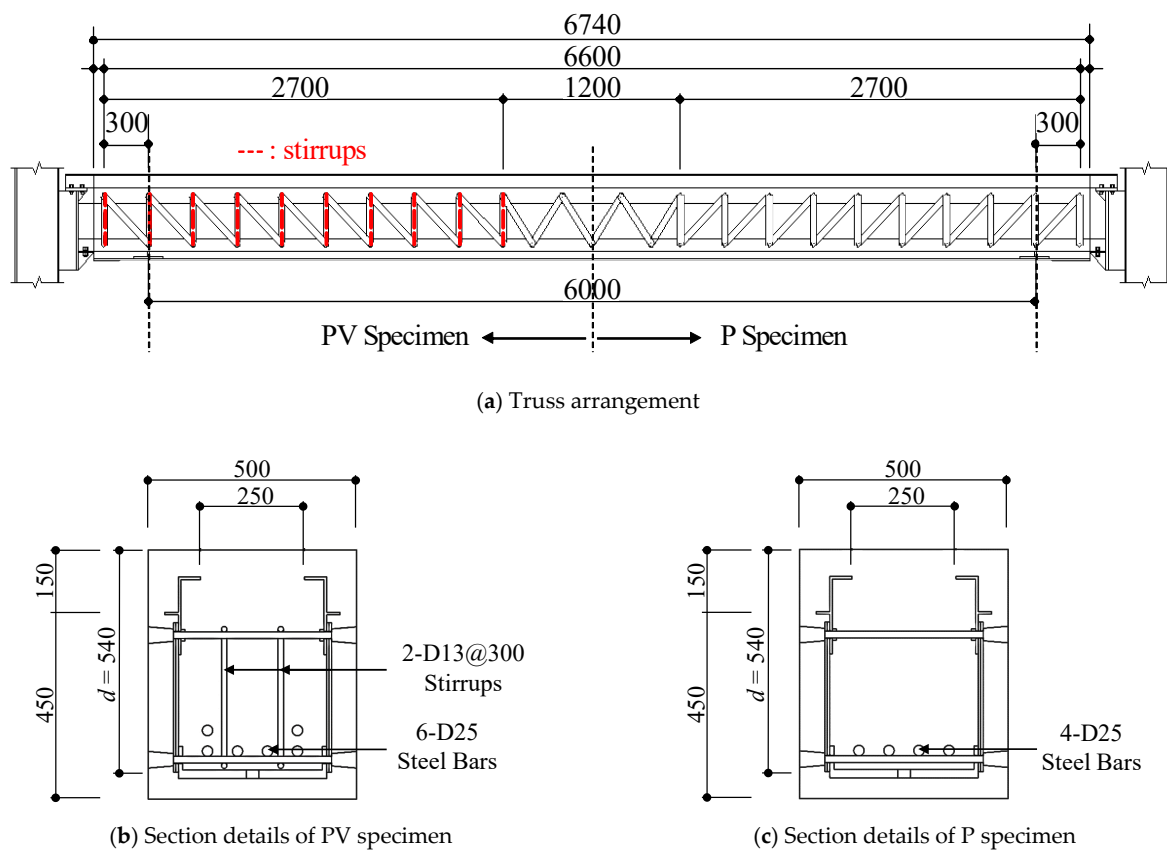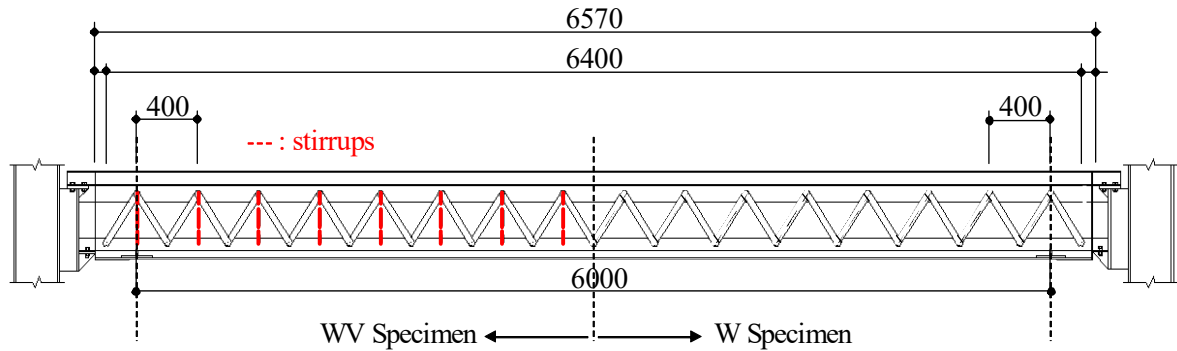(**c**) Section details of P specimen

Figure 3. Dimensional details of P specimen series.

Figure 4 shows the details of the W specimen series (specimen WV, specimen W), to which the Warren truss is applied, and WV and W represent the specimens with and without vertical stirrups, respectively. The thickness of the bottom chord placed on the tension side of the section was 20 mm in the WV specimen and 16 mm in the W specimen. Except for the presence of stirrups and the thickness of the bottom chord, all the section details were the same for both specimens. In addition, the top, bottom, and side cover thicknesses were the same as those of the P specimen series. Figure 5 shows the dimensional details of the top and bottom chords. In the bottom chords, holes with a diameter of 30 mm were drilled at 300 mm intervals such that concrete could be secured tightly on the tension side of the section at the lower end of the bottom chord, preventing air voids.

Note that the purpose of this experimental program was to evaluate the shear strength of EST composite girder. Therefore, all the specimens were designed to have sufficient flexural strengths for inducing shear failure. Detailed calculation process of the flexural strengths of test specimens is presented in the Appendix A. However, the thicknesses of the top chords and the diagonal members of the specimen could not be changed for the fabrication reason. In the end, in this experiment, the flexural strength had to be satisfied only by controlling the cross-sectional area of the tensile reinforcement and the thickness of the bottom chord. Accordingly, some of the details were changed for each test specimen.

Table 2 summarizes the material test results of steel plates and reinforcing bars used for the specimen fabrication. The yield strength of the 13 mm diameter stirrups (f_{vy}) was 465.8 MPa, whereas that of the 25 mm diameter tensile reinforcement (f_y) was 643.0 MPa. Meanwhile, the yield strength of the steel plate (F_y) used in the truss production ranged from 334.1 to 482.0 MPa, and the compressive strength of concrete (f'_c) used in the specimen fabrication was 29.7 MPa. Figure 6 shows the supports and loading points of the specimens. The lengths of the left span (test region) and right span were differently set to 1300 and 3200 mm, respectively, by which the shear force generated in the left shear span was about 2.5 times higher than that in the right shear span; thus, shear failure could be induced

in the left shear span. The shear-span-to-depth ratio (a/d) was set to 2.5, and one-point loading was applied using a universal testing machine with 3000 kN capacity. To measure the deflection of the specimen, a linear variable differential transformer was installed at the loading point as well as in the lower part of the section located in between the loading point and support.
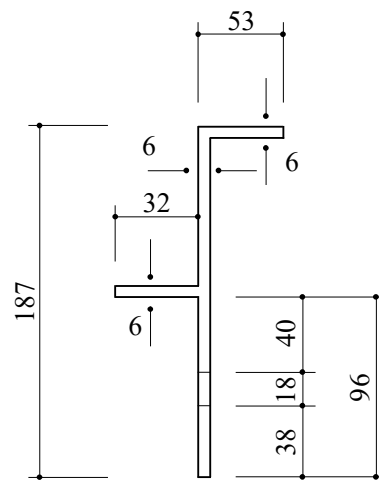

(**a**) Truss arrangement
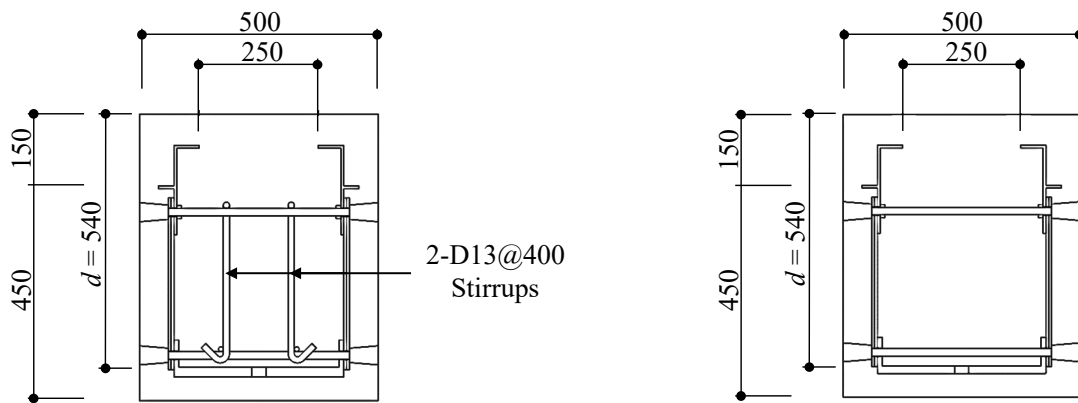
(**b**) Section details of WV specimen

(**c**) Section details of W specimen

Figure 4. Dimensional details of W specimen series.
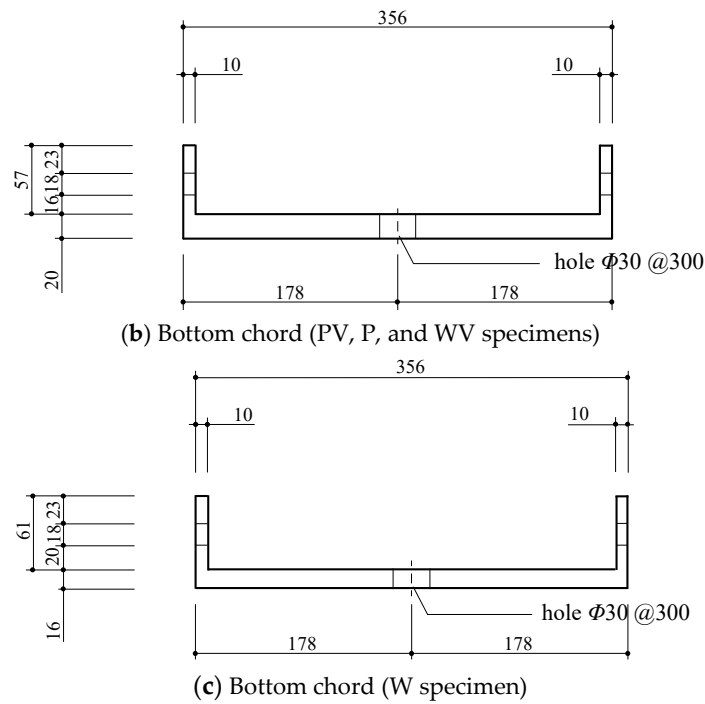

(**a**) Top chord

Figure 5. *Cont.*

(**b**) Bottom chord (PV, P, and WV specimens)

(**c**) Bottom chord (W specimen)

Figure 5. Dimensional details of top and bottom chords.
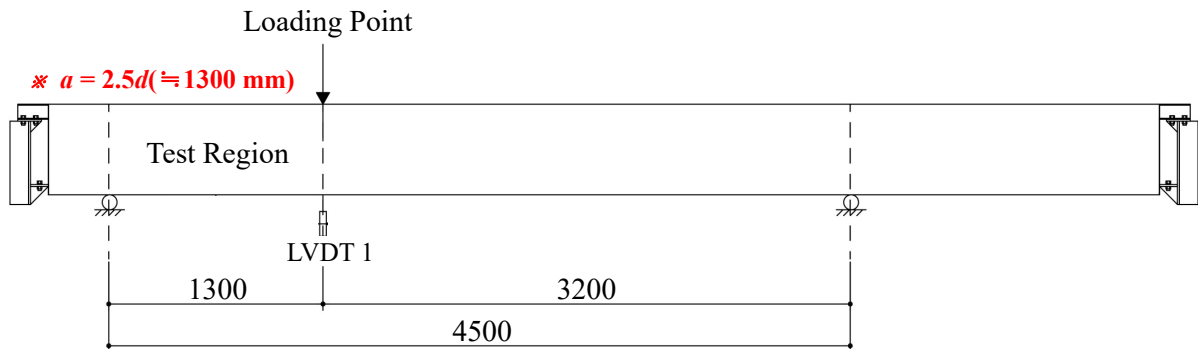
Figure 6. Loading details.

Table 2. Material test results.

		Yield Strength (MPa)	Ultimate Strength (MPa)	Elastic Modulus (MPa)
Reinforcement	D13	465.8	590.7	195,032.9
	D25	643.0	762.6	221,497.5
Steel	Thickness = 6t	482.0	533.0	205,712.0
	Thickness = 10t	352.6	508.1	212,398.3
	Thickness = 16t	355.1	543.4	209,262.0
	Thickness = 20t	334.1	508.1	221,230.3

2.2. Test Results

Figure 7 shows the shear force-deflection relationship of the specimens. As shown in Figure 7a, in the PV specimen with the Pratt truss applied and the vertical stirrup placed, the first flexural-shear cracks occurred at a shear force of 468.7 kN, and web shear cracks were observed at a shear force of 543.6 kN. Even after the web shear cracks appeared, the stiffness decrease in the specimen was insignificant. Meanwhile, at a shear force of

691.6 kN, the specimen underwent failure as horizontal shear cracks occurred along the top chord, as shown in Figure 8a. In the P specimen without a vertical stirrup, flexural-shear cracks appeared at a shear force of 325.9 kN, whereas web shear cracks were observed at a shear force of 421.5 kN. Subsequently, a rapid decrease in stiffness occurred as horizontal shear cracks propagated along the top chord at a shear force of approximately 500 kN. After that point, ductile behavior was observed, followed by the load gradually decreasing after a maximum shear force of 520.5 kN. Even in the case involving the P specimen, it was discovered that horizontal shear cracks that occurred along the top chord led to the dominant failure mode of the specimen, as shown in Figure 8b.
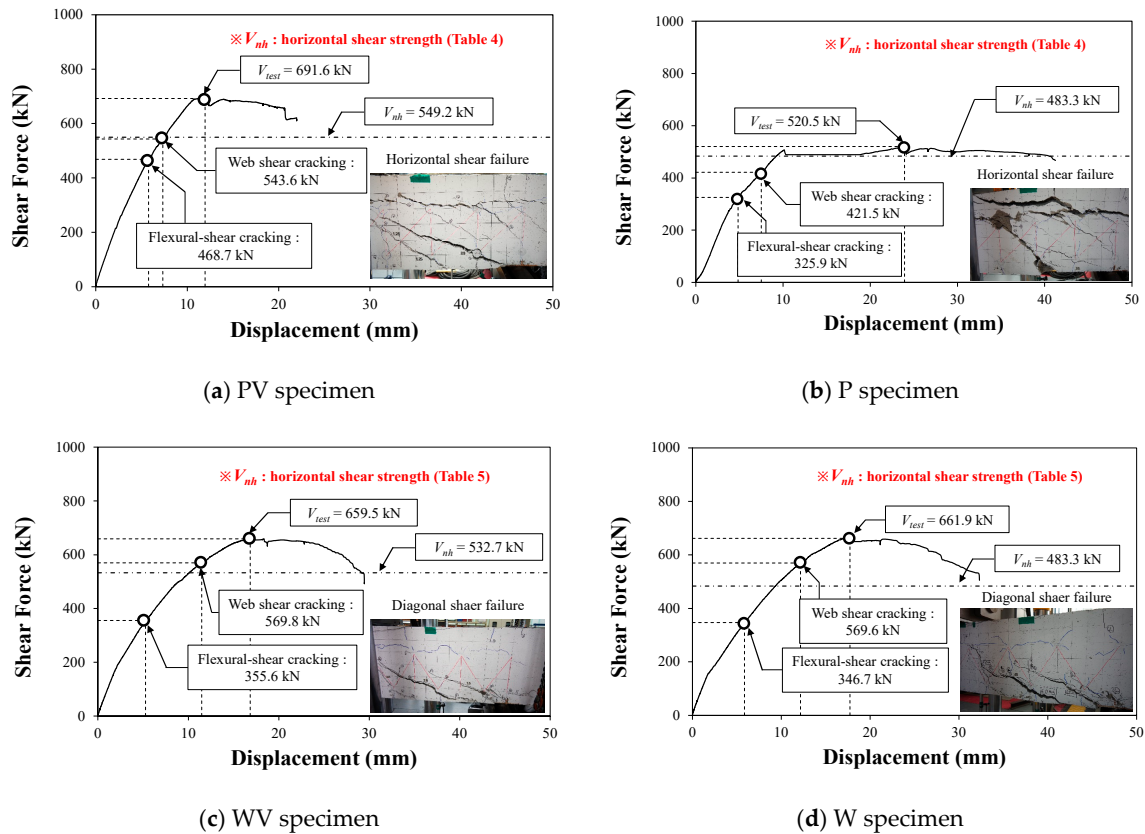

(**a**) PV specimen

(**b**) P specimen

(**c**) WV specimen

(**d**) W specimen

Figure 7. Shear force-deflection response curves of test specimens.

Figure 7c shows the shear force-deflection relationship of the WV specimen with the Warren truss applied and vertical stirrup placed. In the WV specimen, flexural-shear and web shear cracks occurred at shear forces of 355.6 and 569.8 kN, respectively, and the specimen underwent shear failure as the width of the diagonal cracks increased rapidly at a shear force of approximately 659.5 kN, as shown in Figure 8c. Furthermore, the behavior of W specimen without stirrups was very similar to that of the WV specimen, as shown in Figure 7d. In particular, although the stirrup was not placed in the W specimen, the failure mode (i.e., diagonal shear failure) and maximum shear force (661.9 kN) were similar to those of the WV specimen in which the stirrup was placed. The cause can be inferred from the behavior of the diagonal web member of the EST shown in Figure 9. As shown in Figure 9a, the tensile strain of the diagonal member—measured using a strain gauge during the maximum shear force—was 1155 $\mu\varepsilon$, which was approximately 49% of the yield strain (2343 $\mu\varepsilon$) derived from the material test. This implies that in the W specimen series, the diagonal web member failed to fully contribute to the shear resistance. Figure 9b shows the shear failure of the screw rod observed from the EST node area of the W specimen series after the test had completed. It was assumed that as the diagonal web member lost its shear resistance performance due to the damaged screw rod during the test, the W

specimen series underwent premature failure. If the screw rod is affected by shear failure prior to the yielding of a diagonal member, then the diagonal member loses its anchorage performance, and the tensile force is exerted only by the bond between steel and concrete. In general, the bond strength between steel and concrete is extremely small compared with that between deformed bars and concrete. Therefore, when the anchorage at the truss node fails, the shear resistance performance of the diagonal member decreases rapidly, which may result in the brittle fracture of the member. Hence, it was assumed that because of the failure of the screw rod during the test, the stirrup placed in the WV specimen did not effectively contribute to the shear resistance.

(**a**) PV specimen

(**b**) P specimen
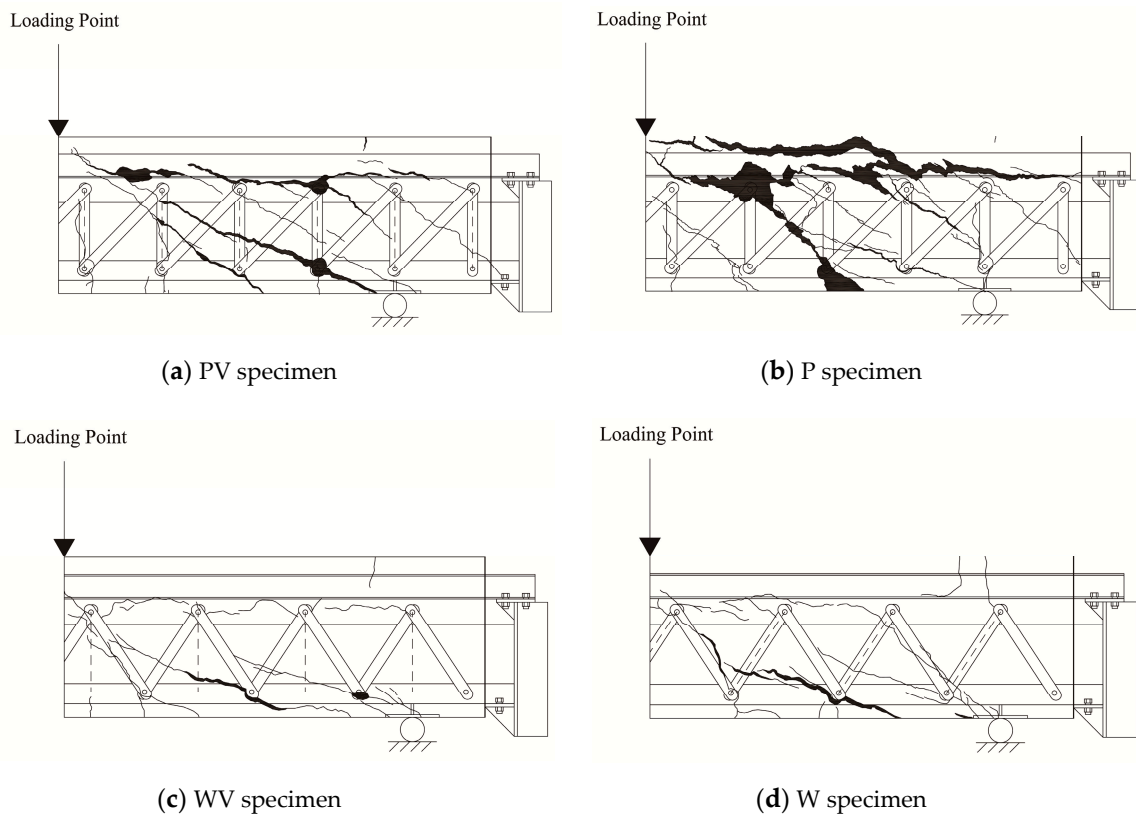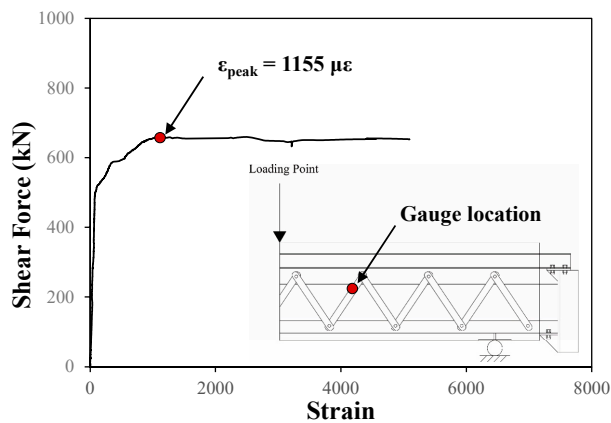
(**c**) WV specimen

(**d**) W specimen

Figure 8. Crack patterns of test specimens at failure.

(**a**) Diagonal web member behavior at critical section

(**b**) Shear failure of screw rod at truss connection

Figure 9. Shear resistance mechanism of web members.

Table 3 summarizes the failure modes and maximum shear forces of each specimen. In the P specimen series applied with the Pratt truss, the dominant failure modes of the specimens were the horizontal shear cracks that occurred along the top chord. Meanwhile, in the W specimen series applied with the Warren truss, no horizontal shear crack was observed, but the anchorage failure of the diagonal web member governed the shear behavior of the specimen.

Table 3. Test results.

Specimen	V_{test} [a] (kN)	Failure Mode
PV	691.6	Horizontal shear failure
P	520.5	Horizontal shear failure
WV	659.5	Diagonal shear failure
W	661.9	Diagonal shear failure

[a] V_{test} = shear strength obtained from test.

3. Analysis and Discussion

3.1. Horizontal Shear Failure

Figure 10 shows the failure surface and resistance area against horizontal shear in the EST composite girder. It is noteworthy that the failure surface due to horizontal shear observed from the shear test was consistent with the area indicated in red in Figure 10, i.e., horizontal shear cracking occurred along the failure surface with the lowest horizontal shear resistance. The horizontal shear strength (V_h), considering the failure surface, can be calculated as follows:

$$V_h = V_{sh} + V_{ch} \tag{1}$$

$$V_{sh} = f_{sc} b_f l_a \tag{2}$$

$$V_{ch} = v_c b_c l_a, \tag{3}$$

where V_{sh} is the horizontal shear strength that can be developed via the bond force of the steel member; V_{ch} is the horizontal shear strength of concrete; f_{sc} is the bond force between steel and concrete, which was set as 0.66 in this study [19]; b_f and b_c are the widths of the steel and concrete surfaces, respectively, within the resistance area for the horizontal shear force; l_a is the length of the shear span; and v_c is the horizontal shear strength of concrete calculated using shear friction theory [20]. The calculated horizontal shear strength (V_h) can be converted to the vertical shear strength (V_{nh}) as follows:

$$V_{nh} = \frac{V_h(jd)}{l_a}, \tag{4}$$

where jd is the length of the moment lever arm. Table 4 shows a comparison of the shear strength (V_{nh}) calculated using Equations (1)–(4) with that obtained from the tests (V_{test}) among the P specimen series. It was discovered that Equations (1)–(4) provided relatively accurate estimations and conservative results for the horizontal shear strength of the specimen. However, because the horizontal shear failure of the member observed in this study was not a desirable failure mode, sufficient horizontal shear strength should be secured by applying Equations (1)–(4) to the design of the EST composite girder.
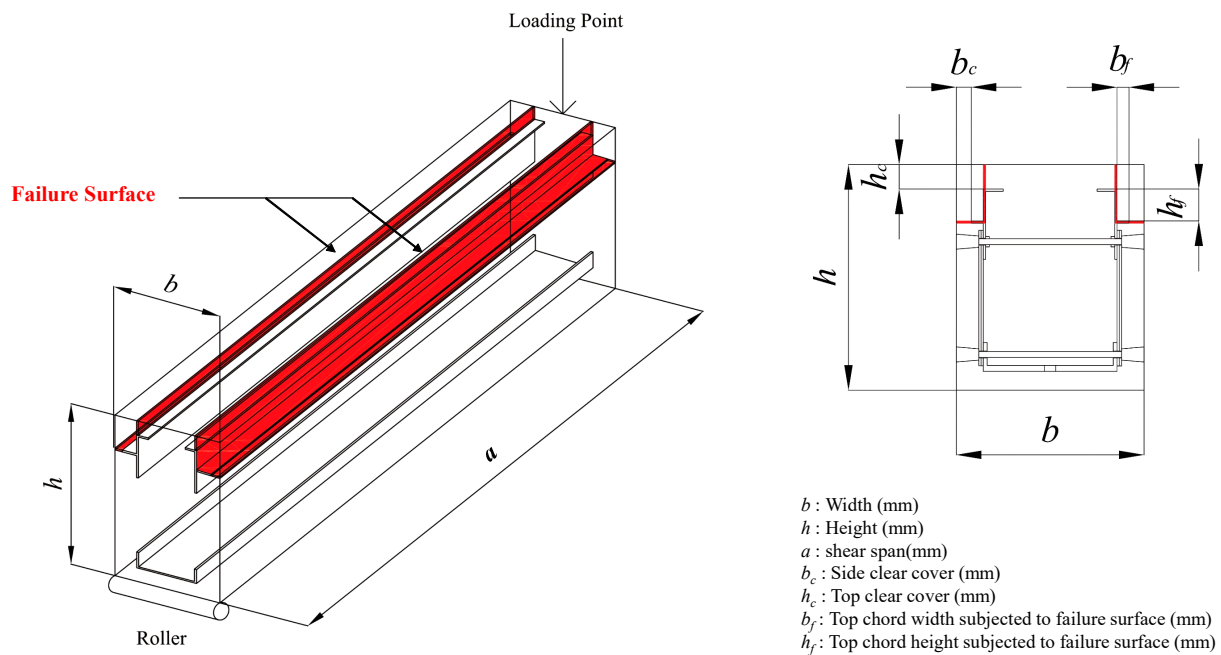
Figure 10. Horizontal shear failure surface.

Table 4. Comparison of test and analysis results on P specimen series.

Specimen	V_{test} [a] (kN)	V_{nh} [b] (kN)	V_{test}/V_{nh}	Failure Mode
PV	691.6	549.2	1.26	Horizontal shear failure
P	520.5	483.3	1.08	Horizontal shear failure

[a] V_{test} = shear strength obtained from test, [b] V_{nh}: calculated horizontal shear strength.

3.2. Shear Failure at Truss Node

As described earlier, in the case of the W specimen series applied with the Warren truss, the diagonal web member failed to exhibit effective shear resistance owing to the shear failure of the screw rod at the EST node. Figure 11 shows a free-body diagram at the Warren truss node. When diagonal cracking occurred, the diagonal web member was subjected to tensile force, and a shear force occurred on the screw rod. The shear strength of the specimen was calculated considering the screw rod failure and then compared with the test results. In this study, the crack angle was assumed to be 45°, and the force of the diagonal member, which was exerted parallel to the crack direction, was disregarded for a simple calculation. In addition, because the bottom plate was fully anchored with bolts at both ends of the member and the bond stress between the steel plate and concrete was extremely small, the tensile force increment (ΔT) of the bottom plate was disregarded as well. Under some assumptions, the tensile force acting on the diagonal web member (T_w) at the instant of the screw rod failure can be expressed as follows:

$$T_w = V_{n,bolt} = 0.6 A_{wn} F_y,\tag{5}$$

where $V_{n,bolt}$ is the shear strength of the screw rod; A_{wn} and F_y are the section area and yield strength of the screw rod, respectively. The shear strength of the screw rod with a diameter of 16 mm and yield strength of 400 MPa was 48.23 kN, as calculated using Equation (5). The stress of the diagonal member (f_s) at the shear failure of the screw rod can be calculated as follows:

$$f_s = \frac{V_{n,bolt}}{A_{s1}},\tag{6}$$

where A_{s1} is the cross-sectional area of one diagonal member. Because the cross-sectional area of the diagonal member placed in the W specimen series was 240 mm^2 (40 mm × 6 mm), the stress of the diagonal member at the shear failure of the screw rod was calculated to be 200.96 MPa. If using the equation for calculating the shear strength specified in ACI 318-19 [20], where the diagonal member is regarded as a stirrup, and the stress of the diagonal member (f_s) calculated using Equation (6) is substituted for the yield stress, then it can be represented by the following equation:

$$V_{sr} = 0.17\sqrt{f'_c} + \frac{A_s f_s d}{s}(\sin\alpha + \cos\alpha), \tag{7}$$

where f'_c is the compressive strength of concrete; A_s and f_s are the section area and stress of the diagonal web member, respectively; s is the spacing of the web members; and α is the angle of the diagonal member. Table 5 shows the shear strengths of the specimens calculated using Equations (5)–(7). The proposed equation only provided an estimation of the shear strength of the specimens. However, it is noteworthy that if the screw rod exhibits shear failure prior to the yielding of the diagonal web member, then a very brittle failure may occur in the member. In this case, a screw rod that is sufficiently large for providing the adequate diameter and strength should be used in designing the EST composite girder. For the Pratt truss specimen in this experimental program, it was discovered that horizontal shear cracks that occurred along the top chord led to the dominant failure mode of the specimen. Based on the test results, it is estimated that the horizontal shear strength of the Pratt truss specimens was less than the shear strength of the screw rods.
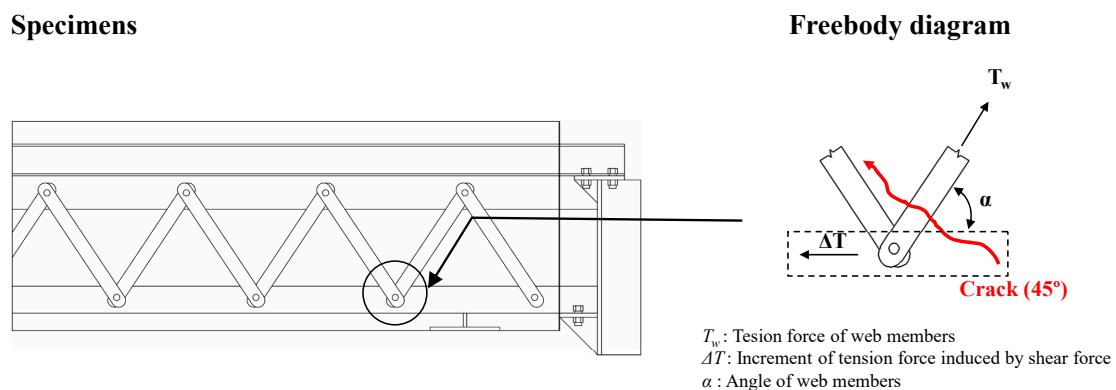
Specimens **Freebody diagram**

T_w: Tesion force of web members
ΔT: Increment of tension force induced by shear force
α: Angle of web members

Figure 11. Freebody diagram at truss connection.

Table 5. Comparison of test and analysis results on W specimen series.

Specimen	V_{test} [a] (kN)	V_{sr} [b] (kN)	V_{test}/V_{sr}	Failure Mode
WV	659.5	655.3	1.01	Diagonal shear failure
W	661.9	515.8	1.28	Diagonal shear failure

[a] V_{test} = shear strength obtained from test, [b] V_{sr}: shear strength considering screw rod failure.

4. Conclusions

In this study, tests using truss type and presence of stirrups as variables were performed to verify the shear performance of EST composite girders. Subsequently, based on the crack patterns and failure modes observed from the tests, the behavioral characteristics of the EST composite girder were analyzed in detail. The following conclusions were obtained from this study:

1. It was discovered that in the P specimen series applied with the Pratt truss, horizontal shear cracks that occurred along the top chord governed the shear behavior of the member. In addition, the shear strength calculation method considering the horizontal

　　　shear failure surface provided relatively accurate and conservative results for the shear strength of the P specimen series.

2. In the W specimen series applied with the Warren truss, the diagonal web member failed to contribute effectively to the shear resistance mechanism of the member. This was because the screw rod exhibited shear failure at the EST node area before the diagonal web member reached its yield strength. Meanwhile, it was discovered that the shear strength calculation method considering the shear failure of the screw rod predicted the shear strength of the W specimen series reasonably well.

3. Horizontal shear failure was one of the main failure modes of encased composite girders, and a very brittle failure may occur in the entire member when the screw rod exhibits shear failure prior to the yielding of the diagonal web member. Therefore, these aspects should be considered when designing an EST composite girder.

4. Some of the shear behavior characteristics of EST composite girders were identified in this study. However, the EST composite girders fabricated in this study did not necessarily exhibit a desirable failure mode. Hence, it is predicted that if the shear failure strength of the screw rod and the horizontal shear strength presented in this study are considered in the design process, then undesirable failure modes can be avoided.

5. There could be a stress concentration at truss nodes, which caused a brittle shear failure of the screw rod. Therefore, a finite element analysis is recommended as a future research work to identify the stress concentration phenomenon. In addition, because the EST composite girder system was designed to allow the beam-column to be continuous in the negative moment region, additional investigations regarding the seismic performance of the EST girder–column connection should be conducted.

Author Contributions: Original draft manuscript, C.L.; validation, S.-H.C. and S.-J.H.; investigation, J.Y.O. and M.-S.L.; supervision and review writing, K.S.K. All authors have read and agreed to the published version of the manuscript.

Institutional Review Board Statement: Not applicable.

Informed Consent Statement: Not applicable.

Data Availability Statement: The data presented in this study are available on request from the corresponding author.

Conflicts of Interest: The authors declare no conflict of interest.

Appendix A

　　　The flexural strengths of test specimens were calculated, as follows:

$$M_n = 0.85 f_{ck} \frac{bc^2}{2} + \sum_{i=1}^{n} A_{tc,i} F_{ytc,i} (c - d_{tc,i}) + \sum_{i=1}^{n} A_{bc,i} F_{ybc,i} (d_{bc,i} - c) + \sum_{i=1}^{n} A_{r,i} f_{yr,i} (d_{r,i} - c) \tag{A1}$$

　　　where b is the width of beam; c is the neutral-axis depth calculated under the assumption of plastic stress distribution; $A_{tc,i}$ and $A_{bc,i}$ are the cross-sectional area of top and bottom chords, respectively; and $F_{ytc,i}$ and $F_{ybc,i}$ are the yield strengths of steel plates used for top and bottom chords, respectively. In addition, $d_{tc,i}$ and $d_{bc,i}$ are depths of top and bottom chords, respectively; $A_{r,i}$ and $f_{yr,i}$ are the cross-sectional area and yield strength of tensile reinforcement at each layer, respectively; and $d_{r,i}$ is the depth of tensile reinforcement at each layer. All the calculated flexural strengths of test specimens using Equation (A1) are summarized in Table A1.

Table A1. Calculated flexural strength.

Specimen	Sectional Area of Reinforcement (mm^2)		Flexural Strength (kN·m)	Shear Force at Reaching Flexural Strength (kN)
	Bottom Chord	**Rebar**		
PV	6520	3036	1524.5	1172.7
P	6520	2024	1424.1	1095.5
WV	6520	-	1080.6	831.2
W	5216	-	926.0	712.3

References

1. Colajanni, P.; Mendola, L.L.; Monaco, A. Experimental Investigation of the Shear Response of Precast Steel–Concrete Trussed Beams. *J. Struct. Eng.* **2019**, *143*, 04016156. [CrossRef]
2. Monti, G.; Petrone, F. Shear Resisting Mechanisms and Capacity Equations for Composite Truss Beams. *J. Struct. Eng.* **2015**, *141*, 04015052. [CrossRef]
3. Kim, K.S.; Lee, D.H.; Choi, S.M.; Choi, Y.H.; Jung, S.H. Flexural behavior of prestressed composite beams with corrugated web: Part I. Development and analysis. *Compos. Part B Eng.* **2011**, *42*, 1603–1616. [CrossRef]
4. Kim, K.S.; Lee, D.H. Flexural behavior of prestressed composite beams with corrugated web: Part II. Experiment and verification. *Compos. Part B Eng.* **2011**, *42*, 1617–1629. [CrossRef]
5. De Sutter, S.; Verbruggen, S.; Tysmans, T. Shear behaviour of hybrid composite-concrete beams: Experimental failure and strain analysis. *Compos. Struct.* **2016**, *152*, 607–616. [CrossRef]
6. Hsu, C.-T.T.; Punurai, S.; Punurai, W.; Majdi, Y. New composite beams having cold-formed steel joists and concrete slab. *Eng. Struct.* **2014**, *71*, 187–200. [CrossRef]
7. Han, S.J.; Jeong, J.H.; Joo, H.E.; Choi, S.H.; Choi, S.D.; Kim, K.S. Flexural and Shear Performance of Prestressed Composite Slabs with Inverted Multi-Ribs. *Appl. Sci.* **2019**, *9*, 4946. [CrossRef]
8. Ayyub, B.M.; Sohn, Y.G.; Saadatmanesh, H. Prestressed composite girders under positive moment. *J. Struct. Eng.* **1990**, *116*, 2931–2951. [CrossRef]
9. Ayyub, B.M.; Sohn, Y.G.; Saadatmanesh, H. Prestressed composite girders. I: Experimental study for negative moment. *J. Struct. Eng.* **1992**, *118*, 2743–2762. [CrossRef]
10. Han, S.J.; Lee, D.H.; Oh, J.Y.; Choi, S.H.; Kim, K.S. Flexural Responses of Prestressed Hybrid Wide Flange Composite Girders. *Int. J. Concr. Struct. Mater.* **2018**, *12*, 1–16. [CrossRef]
11. Oh, B.H. Flexural analysis of reinforced concrete beams containing steel fibers. *J. Struct. Eng.* **1992**, *118*, 2821–2835. [CrossRef]
12. Khuntia, M.; Stojadinovic, B.; Goe, L.S.C. Shear strength of normal and high-strength fiber reinforced concrete beams without stirrups. *ACI Struct. J.* **1999**, *96*, 282–289. [CrossRef]
13. Lim, D.; Oh, B. Experimental and theoretical investigation on the shear of steel fibre reinforced concrete beams. *Eng. Struct.* **1999**, *21*, 937–944. [CrossRef]
14. Yang, I.H.; Joh, C.; Kim, B.-S. Structural behavior of ultra high performance concrete beams subjected to bending. *Eng. Struct.* **2010**, *32*, 478–487. [CrossRef]
15. Yang, I.-H.; Joh, C.; Kim, B.-S. Flexural strength of large-scale ultra high performance concrete prestressed T-beams. *Can. J. Civ. Eng.* **2011**, *38*, 1185–1195. [CrossRef]
16. Yoo, S.-W.; Choo, J.F. Evaluation of the flexural behavior of composite beam with inverted-T steel girder and steel fiber reinforced ultra high performance concrete slab. *Eng. Struct.* **2016**, *118*, 1–15. [CrossRef]
17. Di, J.; Cao, L.; Han, J. Experimental Study on the Shear Behavior of GFRP–Concrete Composite Beam Connections. *Materials* **2020**, *13*, 1067. [CrossRef] [PubMed]
18. Dunaj, P.; Berczyński, S.; Chodźko, M.; Niesterowicz, B. Finite Element Modeling of the Dynamic Properties of Composite Steel–Polymer Concrete Beams. *Materials* **2020**, *13*, 1630. [CrossRef] [PubMed]
19. Structural Korean Ministry of Land Infrastructure and Transportation. *Korean Building Code (KBC 2016)*; Structural Korean Ministry of Land Infrastructure and Transportation: Seoul, Korea, 2016; 937p.
20. ACI Committee 318. *Building Code Requirements for Structural Concrete (ACI 318-19)*; American Concrete Institute: Farmington Hills, MI, USA, 2019; 624p.